JOURNAL OF MATERIALS SCIENCE 22 (1987) 4093–4102

A transmission electron microscope study of a cubic boron nitride-based compact material with AlN and AlB_2 binder phases

J. C. WALMSLEY, A. R. LANG
H. H. Wills Physics Laboratory, University of Bristol, Tyndall Avenue, Bristol BS8 1TL, UK

The microstructure of a commercial cubic boron nitride compact, with aluminium nitride and aluminium diboride binder phases, has been characterized by transmission electron microscopy. Within individual grains significant plastic deformation is observed in the form of dislocations and microtwin lamellae. There is no evidence of recrystallization. Grains have been forced into direct contact, but there is no evidence of new growth of cubic boron nitride between the grains. Some grains have obviously broken or shattered during manufacture. Aluminium nitride is present mostly as an oriented rind around the cubic boron nitride grains where they are not in direct contact, while aluminium diboride forms a largely continuous network in the channels between them. Our observations suggest that the two aluminium compounds are responsible for most of the bonding in the compact. The orientation relationships between the cubic boron nitride and its aluminium nitride rind are, on (1 1 1) facets of BN, BN(1 1 1) ‖ AlN(0 0 0 1) and BN[1 1 0] ‖ AlN[1 1 $\bar{2}$ 0], and on (0 0 1) facets of BN, BN(0 0 1) ‖ AlN(0 0 0 1) and BN[1 1 0] ‖ AlN[1 1 $\bar{2}$ 0]. The aluminium diboride is mostly unoriented. The results are discussed in the context of previous work on diamond-based compact materials.

1. Introduction

Sintered superhard materials (diamond and cubic boron nitride) have been of increasing industrial importance for just over a decade, during which time a wide range of products has become available. Compared with single-crystal products they have the advantage of relative cheapness and, being mechanically isotropic on a macroscopic scale, they are not prone to uneven wear or disastrous cleavage along particular crystallographic directions. Other properties, such as hardness and compressive strength, approach those of single crystals and are far superior to those available in other superhard-material-based composites where diamond or cubic boron nitride grains are embedded in a metal or resin matrix. Cubic boron nitride (cBN) is the second hardest material after diamond and finds application in the hot cutting of iron or nickel-containing workpieces that would chemically attack diamond under the same conditions [1, 2].

The manufacturing process of sintered compacts involves the consolidation of graded powders at pressures and temperatures comparable to those at which they were originally synthesized, that is between 1500 and 2,000° C, and between 50 and 70 kbar (5 and 7 GPa). The high pressure initially encourages densification and causes considerable plastic deformation. The pressure distribution in the compact at this stage is very uneven, being well above the average value where grains are in direct contact and virtually zero elsewhere. Where the diamond and cBN are at pressures at which they are thermodynamically unstable the high temperature causes a significant amount of reconversion to graphite and hexagonal boron nitride (hBN), respectively. Reconversion is mostly restricted to grain surfaces because an overall increase in volume has to be accommodated. Consolidation normally takes place adjacent to a source of a second phase which melts and infiltrates between the grains, sweeping away impurities and either dissolving or reacting with the hBN and graphite that have formed. Thus the final compact consists of a superhard-material polycrystalline network with a binder phase occupying the channels between the grains. It is generally accepted that the binder promotes direct bonding between the grains [1, 2].

With regard to diamond compacts, several TEM studies have been reported [3–6]. These have shown direct evidence of plastic deformation in the form of microtwin lamellae and dislocations. The diamond compacts all contained f c c cobalt as the binder phase. Cobalt is known to be an effective solvent/catalyst for diamond synthesis and during manufacture it dissolves graphite which then reprecipitates as diamond, causing extensive intergrowth of the grains. However, at normal pressures the presence of cobalt at internal diamond surfaces accelerates graphitization at temperatures above about 700° C and leads to degradation of the compact when used above this temperature.

The cBN compact discussed here was consolidated in the presence of aluminium. The residual binder phase is a mixture of aluminium nitride (AlN) and

0022–2461/87 $03.00 + .12

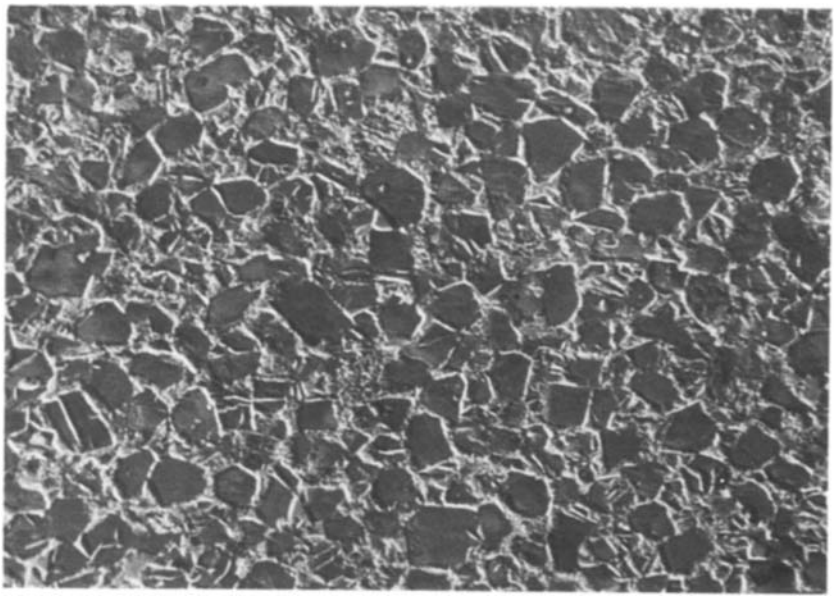

Figure 1 SEM image of Amborite surface after mechanical polishing and then ion-beam bombardment for about 1 h. Field width 90 μm. Individual cBN grains and fragments stand out slightly from the binder phases.

aluminium diboride (AlB_2). These two compounds form a catalytically inactive network that will not encourage the formation of hBN. In addition it protects the internal cBN surfaces from chemical attack, thereby giving excellent thermal stability. The material is marketed under the trade name Amborite*. The AlN content has been measured as ~ 10 wt % and the total binder content as ~ 16 wt % or ~ 18 vol % [7]. Some of the physical properties of the three components of Amborite are listed in Table I.

Amborite is strongly bonded and shows good toughness. Although it is clearly a composite material, its industrially relevant properties, hardness and wear resistance, are derived essentially from the original cBN particles. One motivation for the study here reported was to gain a greater understanding of the nature of the bonding holding the cBN grains in place, given that no solvent/catalyst analogous to cobalt in diamond compacts is present during consolidation.

2. Observations

2.1. Specimen preparation

Our experimental material was standard-grade Amborite which has a grain size of about 8 μm. This was provided in the form of cylinders 3 mm in diameter and several millimetres high. These were spark-cut into circular sections about 1 mm thick which were then mechanically polished down to a thickness of about 50 μm on a cast-iron wheel loaded with diamond powder. Final thinning was achieved by argon ion-beam bombardment from both sides of the specimen, the thinning rate being $\sim 0.5\,\mu m\,h^{-1}$, on each side. Amborite specimens prepared in this way always showed uneven surface topography. Consequently, rather thick areas had to be examined in order to provide a representative section typical of the bulk material. In this respect the availability of a Philips EM430 TEM which can operate at 300 keV, providing greater electron penetration than conventional 100 keV machines, has been a distinct advantage.

2.2. SEM observations

Upon interrupting the ion-beam thinning process after about one hour and examining the specimen surface in a scanning electron microscope the microstructure of Fig. 1 is revealed. Ion-beam milling before micrography has the advantage of removing polishing damage, and it causes the cBN, which appears darker on the micrograph, to stand out a little from the binder phase which etches at a slightly higher rate. Some grains have broken into two or more pieces between which the binder has penetrated. In regions between the larger distinct cBN grains smaller cBN fragments are evident. In some cases these are grouped together in such a way as to suggest that they are remnants of a larger grain that has completely shattered during consolidation. Some may be single fragments from grains that have otherwise remained intact.

2.3. Deformation and other features observed in cBN grains

Fig. 2 shows a transmission micrograph of a cBN

TABLE I Physical properties of the components of Amborite

Compound	Knoop hardness	Melting point (low pressure)	Space group	Morphology	Lattice parameters (nm)	Reference
AlB_2	960 kg mm^{-2} average hardness, 100 g indenter load.	1928 K	P6/mmm	Hexagonal platelets	$a = 0.301$ $c = 0.326$	[8]
AlN	1200 kg mm^{-2} average hardness, 100 g indenter load.	3273 K	$P6_3mc$	Hexagonal platelets	$a = 0.311$ $c = 0.498$	[9]
cBN	7300 to 10 000 kg mm^{-2} hardness	–	$F\bar{4}3m$	Cubo-octahedral	$a = 0.3612$	[9]

*A registered trademark of De Beers Industrial Diamond Division.

Figure 2 A bright-field TEM section through a cBN grain. Field width 6 μm. The grain has [1 1 0] parallel to the beam and [0 0 1] is approximately vertical on the print. White areas on the print correspond to the specimen having thinned right through. Image recorded at 300 kV.

grain tilted to bring the [1 1 0] zone axis parallel to the incident beam. (Micrographs and diffraction patterns in this paper are printed as seen on the fluorescent screen. Thus in the present instance the grain direction [1 1 0] points towards the observer, the direction of the electron beam being [$\bar{1}$ $\bar{1}$ 0]). The image was recorded using a large objective aperture in order to reduce the overall contrast by allowing a significant proportion of inelastically scattered electrons to contribute to the image. The grain section is not complete and the

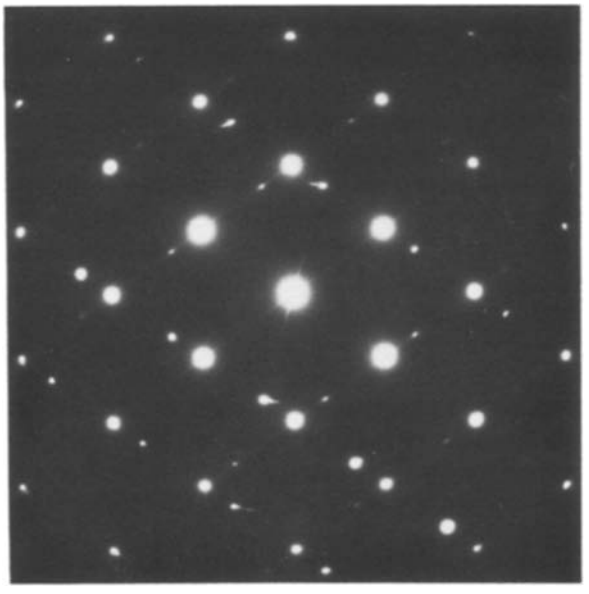

Figure 3 Diffraction pattern from the grain shown in Fig. 2. Weak patterns due to twinning on ($\bar{1}$ 1 1) and (1 $\bar{1}$ 1) are superimposed on the stronger matrix reflections. The ($\bar{1}$ 1 1) set of twin reflections show streaking, parallel to [$\bar{1}$ 1 1], while the (1 $\bar{1}$ 1) set show no streaking. The direction [0 0 1] is vertical on the print. The short streak running through the direct-beam spot, rotated ~ 16° clockwise from vertical, is due to a crack interface parallel to ($\bar{1}$ 1 5) in the left-hand part of the grain.

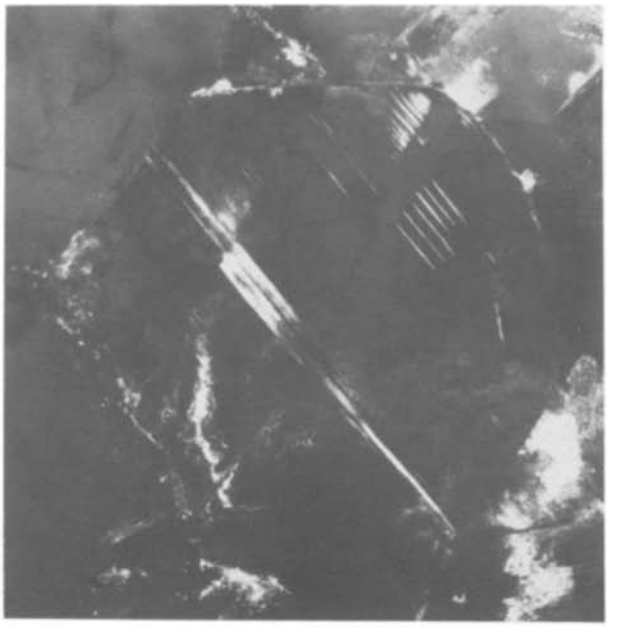

Figure 4 Dark-field image of the same area as Fig. 2, formed by using a 1 1 1-type reflection that is unique to the ($\bar{1}$ 1 1) set of twins.

brightest areas correspond to localities where the specimen has been thinned right through. The dislocation density is high. This is typical although there are large local variations both from grain to grain and within individual grains. Two sets of deformation bands, comprising both slip bands and microtwin lamellae lying parallel to ($\bar{1}$ 1 1) and (1 $\bar{1}$ 1), are viewed edge-on in this orientation. One broad band belonging to the latter set clearly runs the whole width of the grain from top left to lower right. Three cracks (light on print) can be seen associated with the grain, two within the grain and one running round the upper part of its circumference. The appearance of such cracks, which are common after thinning, is attributed to the release of local elastic stresses in the specimen.

A selected-area diffraction pattern from part of the

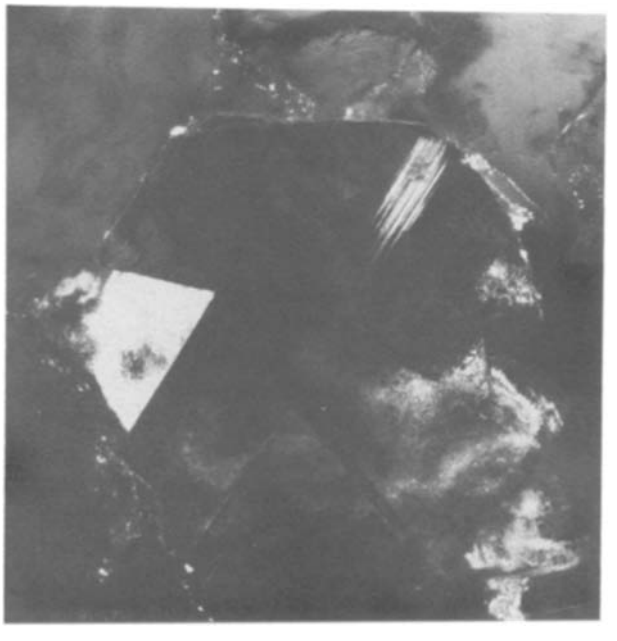

Figure 5 Dark-field image of the same area as Fig. 2, formed using a 1 1 1-type reflection that is unique to the (1 $\bar{1}$ 1) set of twins.

Figure 6 A point of direct contact between two cBN grains. Field width 1.6 μm. The lower left-hand grain is that shown in Fig. 2. Microtwin and slip traces are visible in it. On thinning, the boundary between the two grains has separated slightly.

Figure 7 The edge of a cBN grain, with [1 1 0] approximately parallel to the beam. Field width 0.8 μm. The AlN rind runs diagonally across the field from lower left to top right and is about 20 nm thick except for nodules about 60 nm thick. A defect-free region of the AlB_2 network, appearing light on the print, occupies the lower right-hand part of the field.

grain is shown in Fig. 3. Two sets of twin reflections are present. Reflections due to twins on $(\bar{1}\,1\,1)$ are noticeably elongated in the $[\bar{1}\,1\,1]$ direction and show streaking along all rows in the main diffraction pattern that are parallel to $[\bar{1}\,1\,1]$. The intensity in the streaks can be attributed to the thinner microtwins and the slip bands. A dark-field micrograph, Fig. 4, imaged from one of the diffracted beams due to twinning on $(\bar{1}\,1\,1)$, demonstrates that a large number of microtwin lamellae are present in the main deformation band. Lower densities of lamellae are present in other parts of the grain. On close examination the thinnest twins show a thickness of 10 nm or less. Streaking and elongation of the $(1\,\bar{1}\,1)$ twin reflections is not so evident. Fig. 5 shows a dark-field image formed from one of the $(1\,\bar{1}\,1)$ twin reflections and again some microtwins are visible. There is also a larger area in twin orientation. This is a growth twin that appears to be bounded on two sides within the grain by its own octahedral surfaces. One of the cracks evident in the bright-field micrograph (which is the cause of a short spike running through the direct-beam spot of the selected-area diffraction pattern in Fig. 3) has opened up along the twin boundary that does not correspond to an octahedral facet in both twinned and untwinned material. It can be calculated that this corresponds to a $(\bar{1}\,1\,5)$ composition plane in the parent grain.

The lattice defects introduced into cBN by plastic

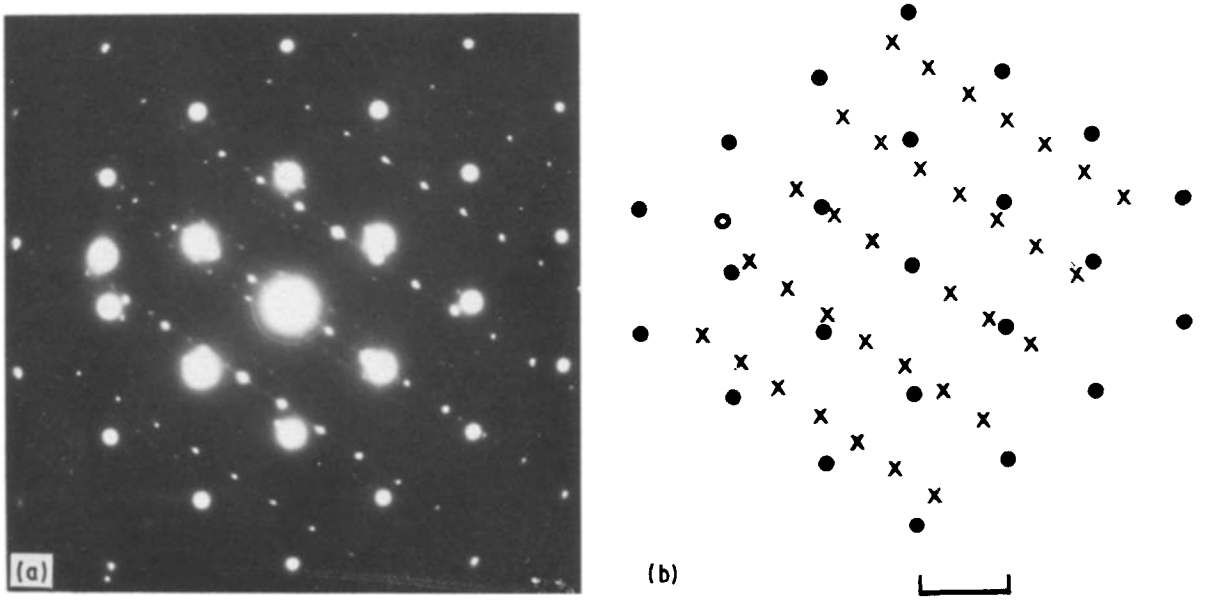

Figure 8 (a) Diffraction pattern showing the relative orientation of the three phases present in Fig. 7. The pattern is in a similar orientation to Fig. 7. Extra rows of spots lying parallel to $[\bar{1}\,1\,1]$ are due to double diffraction. (b) Identification of principal components of pattern in (a): (●) cBN, (○) AlB_2, (x) AlN. Scale mark 4 nm^{-1}.

Figure 9 Dark-field image formed with an AlN reflection showing central part of the AlN rind along the grain edge in Fig. 7a. Field width 0.6 μm, printed rotated 55° clockwise with respect to Fig. 7; the AlN [0 0 0 1] direction is now vertical. Contrast in the AlN is highly uneven.

deformation appear virtually identical to those that have been observed in diamond during the study of diamon-based compacts [6]. The dislocation density is generally so high that individual dislocations cannot easily be resolved. Where the level of deformation is lower, dislocations are observed with Burgers vectors of $\frac{1}{2}\langle 1\,1\,0\rangle$-type. They lie preferentially along $\langle 1\,1\,0\rangle$ directions but very commonly follow curved paths, particularly when they interact with other dislocations. Microtwins in the cBN of Amborite exhibit the same distribution as those in diamond compacts [6]. Where two twin lamellae lying on different planes meet in the field of Fig. 2 one of the pair will generally terminate. However, such twin lamellae are often seen to be continuous across an intersection in cBN grains, as is also observed in diamond compacts [6]. No detailed observations of these non-conservative twin intersections in cBN have been made in this study, other than to confirm that they do occur in plastically deformed grains.

2.4. Bonding and the distribution of AlN and AlB_2

Fig. 6 is a higher-magnification view of one corner of the grain shown in Fig. 2 and includes part of an adjacent grain. The specimen is oriented so that both grains give some diffraction contrast. The two grains appear to have mutually indented each other, both showing signs of increased plastic deformation surrounding the point of contact. When examined by TEM, AlN and AlB_2 are found around free edges of the grain sections. The distribution of these two compounds is quite characteristic of the material.

The micrograph of a cBN grain shown in Fig. 7 represents a section normal to an approximately octahedral facet so that the latter is viewed edge-on. Forming a rind at the cBN surface is a thin layer of AlN that appears to be continuous in this field and at several points along its length has developed to form distinct nodules. The central nodule is associated with a "tail" of dislocations in the cBN, extending towards the upper left of the field. They probably constitute a low-angle boundary that would provide an enhanced diffusion route for boron and nitrogen to the grain surface. Outside the AlN is a thicker layer of AlB_2, showing much weaker contrast than the other two phases. Fig. 8a is a selected-area diffraction pattern obtained by including all three phases within the aperture. It comprises a basic [1 1 0] cBN zone axis pattern with a rectangular AlN [1 1 $\bar{2}$ 0] pattern superimposed, and one strong reflection from the AlB_2. The AlN has grown with its (0 0 0 1) basal planes parallel to the cBN (1 1 1) facet plane. Fig. 8b is a key to identification of the principal reflections in Fig. 8a. A dark-field image, Fig. 9, shows that the AlN has a platy morphology beneath the nodules, with a mosaic range of orientation, manifested by uneven contrast. The AlB_2 layer around this grain is comparatively unstrained and dislocation-free. In Amborite the AlB_2 almost always possesses a high degree of crystalline perfection and shows little sign of having been deformed. This is because it grows independently in the liquid aluminium, and by the time it fully occupies the channels between the cBN grains and becomes a rigid network the shape of the compact is largely stable and very little further deformation takes place. Individual crystallites in the AlB_2 network extend to several micrometres in maximum dimensions. AlB_2 penetrates the spaces between the cBN grains completely, leaving no voids or cavities. In addition, no unreacted aluminium was detected in the compact, which suggests that the manufacturing process is well controlled.

A relatively lightly-deformed area of cBN, representing the corner of a grain that has been tilted so that both an octahedral and a cube facet are viewed edge-on, is shown in Fig. 10. A moderate number of dislocations are present. A second cBN grain edge,

Figure 10 Part of the edge of a cBN grain where a cube and an octahedral facet are viewed edge-on. Field width 1 μm. The grain has [1 1 0] approximately parallel to the beam and [0 0 1] is vertical on the print. A neighbouring cBN grain is visible in the lower right corner of the field. Both grains have an AlN rind and the region between rinds is occupied by AlB_2. Arrows point along the interface between AlN and AlB_2 in the lower right of the field. Image recorded at 300 kV.

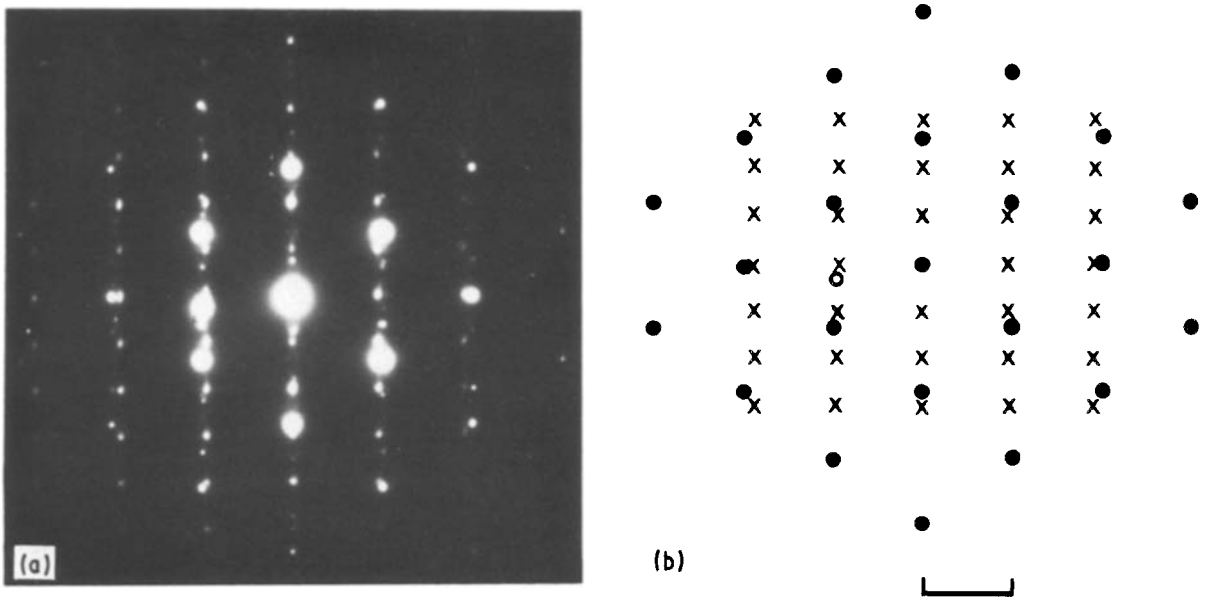

Figure 11 (a) Diffraction pattern showing the relative orientation of the three phases present at the cube facet of the oriented grain in Fig. 10. (b) Identification of the principal components of pattern in (a). (●) cBN, (○) AlB_2, (x) AlN. Scale mark $4\,nm^{-1}$.

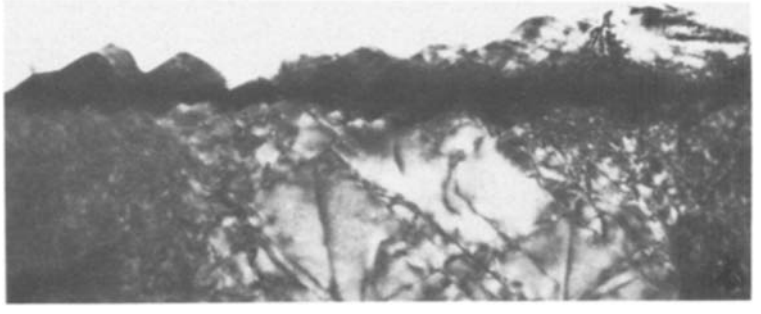

Figure 12 A cBN edge that does not represent a cube or octahedral facet. Field width 1.4 μm. The beam direction is parallel to [1 1 0] and [0 0 1] is horizontal on the print. Individual crystallites of the AlN rind exhibit well-developed (0 0 0 1) faces. Image recorded at 300 kV.

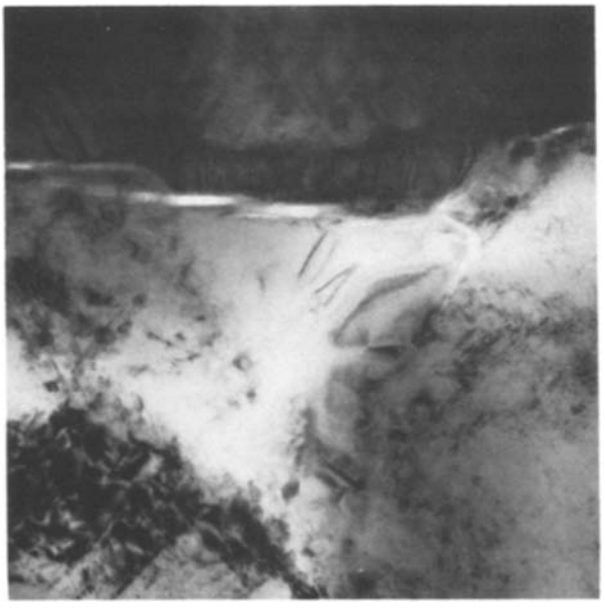

Figure 13 Oriented AlB_2 at the edge of a cBN grain. Field with 1 μm. The cBN grain in the upper part of the field of view has [1 1 0] parallel to the beam and the direction [0 0 1] is vertical on the print. A crack, which has opened on thinning, separates the upper grain from the two out-of-contrast grains below it and from most of the triangular region of AlB_2 that occupies the centre of the field. Image recorded at 300 kV.

well away from any zone axis orientation, is visible in the lower right corner of the field and the gap between the two cBN grains is occupied by the two aluminium compounds. The outline of two slab-like nodules of AlN, which are not showing diffraction contrast, can be seen lying parallel to the surface of the second grain because of Fresnel fringe contrast that is caused by a slight defocus. In this region, a thin oriented rind of AlN is present on both facets of the first grain, and AlN nodules (dark in print) are also present on these facets. The orientation relationship between the AlN and cBN at the octahedral facet is the same as that illustrated in Fig. 8. Fig. 11 shows the relative orientation of the cBN and AlN phases at the cube facet; in this case the basal planes of AlN remain parallel to the new facet plane in the cBN and the AlN $(1\,0\,\bar{1}\,0)$ and cBN (1 1 0) planes normal to the interface are parallel.

At cBN grain surfaces that are not good cube or octahedral facets, such as those produced by irregular growth or by cracking during densification, an AlN rind will still grow with crystallographic directions and planes parallel to those of the cBN. The orientation is not always as exact as it is found to be on a well-defined cBN facet. The orientation relationship AlN$(0\,0\,0\,1)$ ‖ cBN$(1\,1\,1)$ and AlN$[1\,1\,\bar{2}\,0]$ ‖ cBN$[1\,1\,0]$ (i.e. that of Fig. 8) is found to be much the most

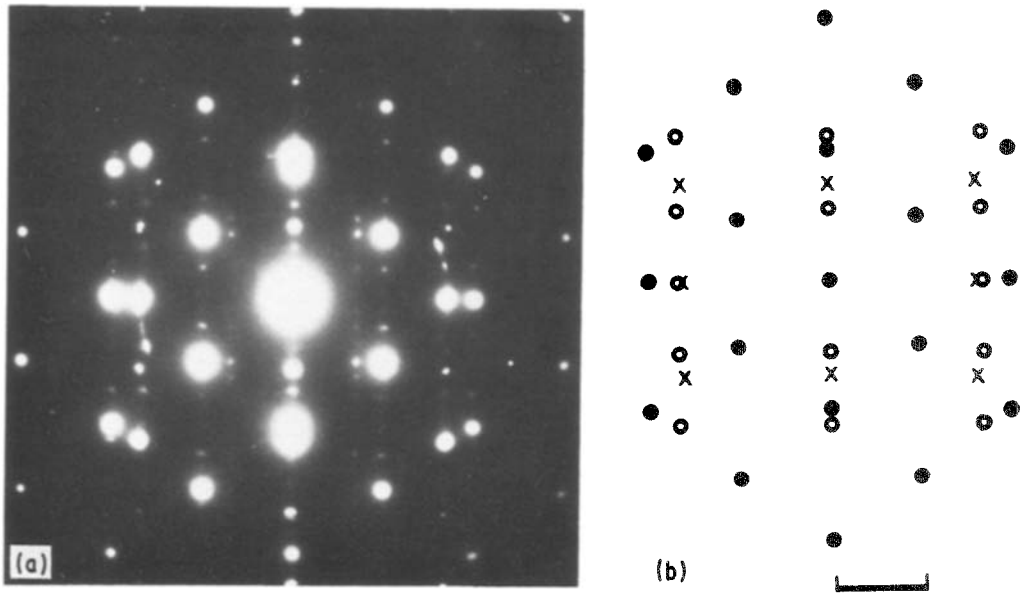

Figure 14 (a) Diffraction pattern showing the relative orientation of phases at the edge of the upper grain in Fig. 13. The main reflections are identified in (b). Subsidiary spots are due to double diffraction. (●) cBN, (○) AlB_2, (x) AlN. Scale mark $4\,nm^{-1}$.

common. The preference for this particular orientation is plausible given that the hexagonal arrangements of nitrogen atoms in the basal plane of AlN and in the cBN octahedral plane are virtually identical [10]. In the absence of well-developed cBN facets the AlN still tends to form small plate-like crystallites whose surface normal is parallel to cBN[1 1 1]. The underlying cBN is then usually {1 1 1} faceted on a fine scale (~ 20 nm). The situation is illustrated in Fig. 12. There the mean trace of the cBN grain edge is close to $(1\,\bar{1}\,0)$ and it is likely that the original grain had a roughly $(1\,\bar{1}\,0)$ surface that was attacked by the aluminium. The diffraction pattern (not reproduced here) shows that the segment of AlN rind in this field has its basal plane rotated about 4° off parallelism with one set of octahedral facets on the cBN grain.

The orientation relationships between AlN and cBN so far discussed account for most of the boundaries at cBN grain surfaces. However, another configuration, involving cBN, AlN and AlB_2, occurs comparatively rarely, and is illustrated in Figs 13 to 16. Here the AlB_2 crystallizes with $AlB_2(0\,0\,0\,1)$ planes parallel to a cBN(0 0 1) facet plane, and $AlB_2(1\,0\,\bar{1}\,0)$ and cBN(1 1 0) are parallel. A thin layer of AlN, having basal planes parallel to the cube facet plane, lies between the AlB_2 and cBN. The relative orientation of the phases is demonstrated by the diffraction pattern, Fig. 14, produced by the upper half of the field of Fig. 13. The dark-field images, Figs 15 and 16, show the distribution of the aluminium compounds.

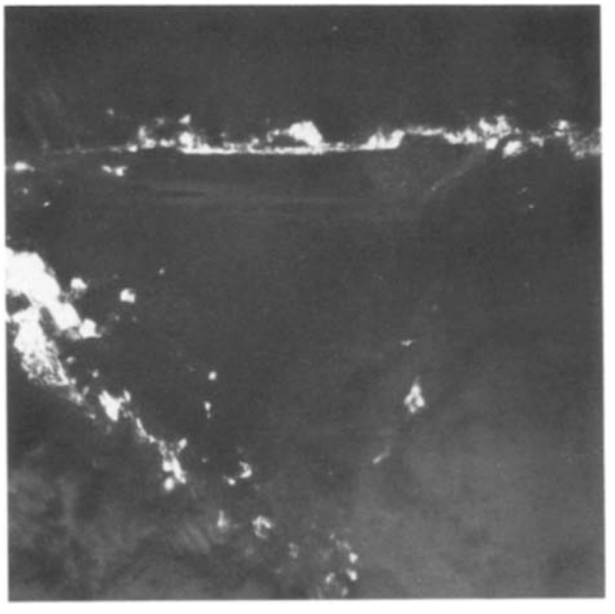

Figure 15 Dark-field image from the same area as Fig. 13, using a 0 0 0 2-type reflection from the thin AlN layer around the cBN grain. Some contrast is present from the AlN around the two neighbouring cBN grains.

Figure 16 Dark-field image from the same area as Fig. 13, formed using an AlB_2 reflection. The AlB_2 that has remained attached to the upper grain is in strong contrast while the rest has become slightly misoriented and does not show such strong contrast. It can be presumed that most of the AlB_2 in the cavity between the three cBN grains had the orientation illustrated in Fig. 14 before the specimen was thinned.

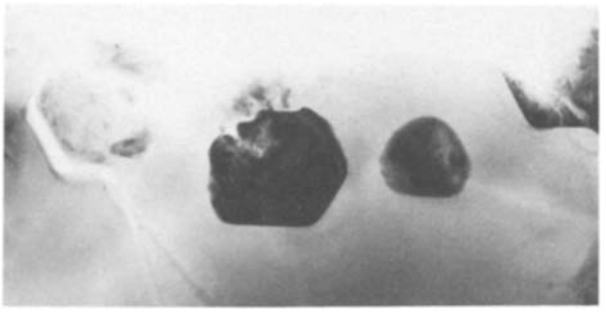

Figure 17 Two single-crystal inclusions of AlN embedded in the AlB_2 network. Field width 0.75 μm. Image recorded at 120 kV.

The AlB_2 here originally crystallized in a cavity between three cBN grains brought into contact during densification, and on thinning it has separated into several fragments.

Inclusions of AlN are sometimes observed embedded in the AlB_2 network, remote from the cBN. Fig. 17 shows two such inclusions the larger of which is in [0 0 0 1] zone-axis orientation. Neither has a simple crystallographic orientation relationship with the surrounding AlB_2. Possibly these inclusions broke away from a cBN surface after nucleation, but it is more likely that they are derived from small pieces of cBN or hBN that have reacted completely with aluminium.

2.5. The fragmentation of cBN grains during densification

Fig. 18 shows several cBN fragments that certainly derive from the same original crystal. They lie between three large, unfragmented cBN grains which enter the upper right, bottom right and lower left marginal areas of the field. The gaps between cBN fragments have been penetrated by aluminium and occupied by its reaction products. The specimen is fairly thick so that some of the cBN fragments are overlapped by the binder phases and the beam in places is passing through two or more layers of different composition. Three fragments are particularly distinct, appearing rather light on the print because they are weakly diffracting. They extend through the full specimen thickness. Around some segments of their edges the AlN rind is discernible. The AlB_2 has crystallized between the fragments in one overall orientation although the dark-field image formed from an AlB_2 reflection (Fig. 19) does not show even contrast throughout due to distortions. Some patches of the AlB_2 network are very strongly diffracting and hence appear completely white on the dark-field image print, while others that are well away from a diffraction condition contain "pseudo-weak-beam" dislocation images and thickness fringes.

Frequently the deformation and shattering of cBN produces areas where the compact is polycrystalline on a much finer scale than that of the starting material or even that represented by Fig. 18. The diffraction pattern Fig. 20 was obtained from the central part of such an area about 5 μm across, and it shows rings due to the presence of cBN and AlN. No AlB_2 was detected in the area. This is probably because the total surface area of cBN that was exposed to aluminium was so large relative to the local interstitial volume that all the spaces between cBN fragments had been fully occupied by AlN before any AlB_2 started to crystallize. The (1 1 1) and (2 2 0) cBN rings in the pattern include short arcs containing some discrete reflections, corresponding to a heavily distorted [1 1 0] zone-axis pattern. This indicates that, as well as shattering, at least some of the original cBN in the area has undergone very severe plastic deformation, even more so than is typical in the large, more complete, cBN grains described earlier. The presence of massively deformed cBN fragments in such areas is confirmed by bright-field and dark-field images.

These observations are broadly consistent with the SEM observations made earlier. The majority of the cBN grains survive the compaction process largely intact, but fracture is clearly an important part of the densification process and the presence of cBN fragments distributed in the binder phase of the final

Figure 18 A region occupied by fragments of cBN derived from the same original grain. Field width 4.5 μm. The fragments show varying degrees of plastic deformation. Image recorded at 300 kV. The location of the three weakly diffracting cBN fragments referred to in the text are, with respect to the field centre, lower right, below and upper left. The completely white area towards the bottom of the field is a hole in the specimen.

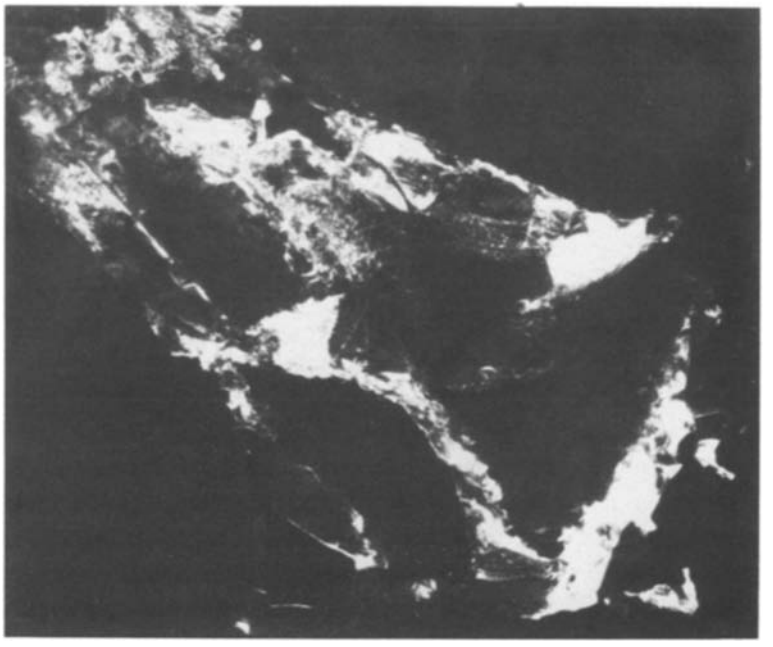

Figure 19 Dark-field image from the same area as Fig. 18, showing the distribution of AlB_2 in between the cBN fragments.

compact is likely to affect its mechanical properties to a certain extent.

3. Conclusions and discussion

The uneven thinning encountered during specimen preparation is a severe obstacle in the study of polycrystalline superhard materials by TEM. However, by observing thicker areas, from which good diffraction information can be obtained, and by examining smaller thin areas in closer detail, some useful results have been obtained from Amborite.

Shattering and plastic deformation of the cBN grains under the application of high pressure provide the mechanism for the densification of the starting material during manufacture. Most of the fracture and breaking-up of grains probably takes place early on in the compaction process and occurs in regions of very high stress. The result is a load-bearing network of cBN grains in which the applied load is supported more evenly than it was in the more loosely arranged starting material. Each grain in this network is constrained by being in contact with several neighbouring grains, and the whole network deforms plastically until densification is complete and no more deformation can be achieved under the applied load. SEM examination of loose cBN grains of the type used as starting material in the manufacture of Amborite confirmed the predominance of good octahedral and cubic facets, although a significant proportion of surfaces are irregular. Some crystals have a "skeletal" morphology and would be very prone to fracture during compaction.

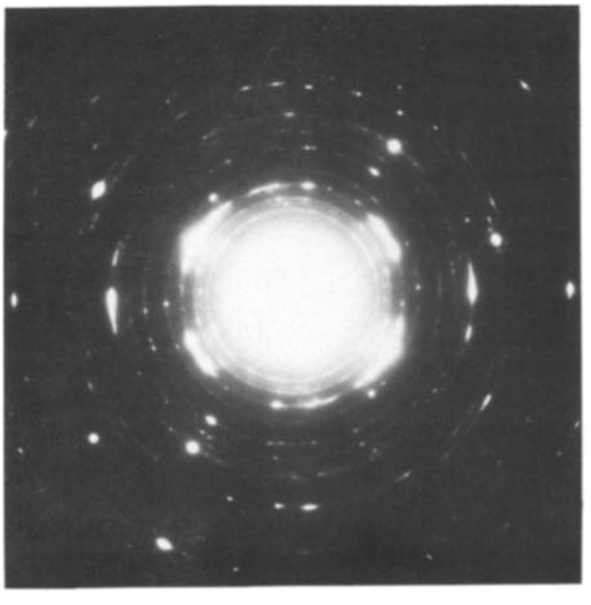

Figure 20 Diffraction pattern from an area containing highly fragmented and deformed cBN together with AlN. Counting from the pattern centre, the first three rings are AlN reflections $1\,0\,\bar{1}\,0$, $0\,0\,0\,2$ and $1\,0\,\bar{1}\,1$. The fourth ring is cBN reflection $1\,1\,1$.

As the aluminium melts and penetrates the channels between the load-bearing cBN network it reacts with the cBN surfaces and any hBN that has developed on them, forming an oriented solid rind of AlN that is continuous except where the grains are protected by being in direct contact with each other. AlB_2 forms in the aluminium by its reaction with liberated boron and eventually produces a continuous polycrystalline skeleton between the cBN grains. Inclusions of AlN found in the AlB_2 network may have been formed by the complete reaction of isolated cBN or hBN fragments with the aluminium.

Our observations are consistent with no crystallization of cBN from solvent/catalyst having taken place during the compaction process to effect intergrowth between cBN grains. The use of AlN as a solid-state catalyst for the conversion of hBN to cBN has been reported [11]. However, in the case of our material all free hBN is likely to be removed by reacting with the aluminium, and not be available for reconversion to cBN. The area of direct contact between cBN grains is such that a significant degree of the bonding and coherence is provided by the aluminium binder phases. Efficient densification by high pressure and consequent production of a load-bearing network of cBN grains in direct contact is clearly a

beneficial factor. However, the compact behaves as a true composite material in which the properties of the binder-phase components and their fine-scale distribution and orientation relationships discoverable by TEM are of major importance.

Acknowledgements

We thank our colleague, Dr R. Vincent, for continuous helpful advice, and Dr R. Caveney, De Beers Industrial Diamond Division (Pty) Ltd, for providing specimens and stimulating investigation of the phenomena studied.

References

1. R. H. WENTORF, R. C. DeVRIES and F. P. BUNDY, *Science* **208** (1980) 873.
2. P. N. TOMLINSON and R. J. WEDLAKE, in Proceedings of the International Conference on Recent Developments in Specialty Steels and Hard Materials, Pretoria, 1982, edited by N. R. Comins and J. B. Clark (Pergamon, Oxford, 1983) p. 173.
3. S. YAZU, T. NISIKAWA, T. NAKAI and Y. DOI, in Proceedings of the International Conference of Recent Developments in Specialty Steels and Hard Materials, Pretoria, 1982, edited by N. R. Comins and J. B. Clark (Pergamon, Oxford, 1983) p. 449.
4. M. LEE, R. C. DeVRIES and E. F. KOCH, G. E. Report No. 84CRD241 (1984).
5. J. C. WALMSLEY and A. R. LANG, *J. Mater. Sci. Lett.* **2** (1983) 785.
6. *Idem*, in "Ultrahard Materials Application Technology," Vol. 3, edited by Paul Daniel (DeBeers Industrial Diamond Division, Ascot, 1985) p. 11.
7. R. J. CAVENEY, private communication (1986).
8. J. A. KOHN, in "Boron, Synthesis, Structures and Properties", edited by J. A. Kohn, W. F. Nye and G. K. Gaulé (Plenum, New York, 1960) p. 75.
9. Landolt-Börnstein Numerical Data and Functional Relationships in Science and Technology, Group III **17**a, edited by O. Madelung (Springer, Berlin, 1982) pp. 148–149, 158–160.
10. S. I. HIRANO, S. HON and S. NAKA, in "High Pressure in Research and Industry" Proceedings of the 8th AIRAPT Conference and 19th EHPRG Conference, Uppsala, 1981, edited by C.-M. Backman, T. Johannisson and L. Tegnér (Arkitektkopia, Uppsala, 1982) p. 376.
11. A. R. BADZIAN and T. KIENIEWICZ-BADZIAN, in "High Pressure Science and Technology" Proceedings of the 7th AIRAPT Conference, Le Creusot, 1979, Vol. 2, edited by B. Vodar and Ph. Marteau (Pergamon, Oxford, 1980) p. 1087.

Received 8 January
and accepted 1 April 1987